Journal of Structural Geology 30 (2008) 1603–1613

Contents lists available at ScienceDirect

Journal of Structural Geology

journal homepage: www.elsevier.com/locate/jsg

Combined kinematic and paleostress analysis of fault-slip data: The Multiple-slip method

Jure Žalohar*, Marko Vrabec

Department of Geology, Faculty of Natural Sciences and Engineering, University of Ljubjana, Aškerčeva 12, SI-1000 Ljubljana, Slovenia

ARTICLE INFO

Article history:
Received 26 November 2007
Received in revised form
12 September 2008
Accepted 12 September 2008
Available online 2 October 2008

Keywords:
Fault-slip analysis
Kinematic analysis
Paleostress analysis
Moment tensor summation

ABSTRACT

We describe the Multiple-slip method for the construction of the displacement gradient tensor, which describes the faulting-related deformation of the region. Three elements must be known for each fault: (1) the fault plane orientation, (2) the slip direction, and (3) the number of parallel faults in the same size range. The data on the orientation of faults and the direction of slip along them define the geometric moment tensor for each fault, while the data on the number of parallel faults belonging to a particular fault-set constrain the weighting factor for each fault. In the Multiple-slip method, the weighting factors also depend on the stress state that produced the displacement along the faults. The stress state on the observed faults at the time of faulting can be estimated from the paleostress analysis, which finds the stress tensor capable of explaining the slip direction along the faults. Therefore, the Multiple-slip method is a combination of kinematic and paleostress techniques, in which the paleostress analysis must be performed prior to the kinematic analysis. The Multiple-slip method allows for calculating (1) the direction of kinematic axes (directions of maximum shortening and extension), (2) the direction and relative magnitude of rotation, and (3) the ratio between the principal strains.

1. Introduction

The net result of a large number of distributed slip events on faults in the Earth's crust is a quasi-continuous deformation referred to as *cataclastic flow* or *fault strain* (Cladouhos and Allmendinger, 1993; Twiss and Unruh, 1998). The first attempts to quantify this faulting-related strain were carried out by Oertel (1965) and Freund (1970). Reches (1978, 1983) developed mathematical theory for describing faulted medium as a continuum and introduced tensor notation. This theory became the basis for the *kinematic analysis* of faults, which allows reconstruction of the principal characteristics of faulting-related strain from measurements of the orientation of fault planes and the direction of slip along them (fault-slip data). A similar approach was developed by Kostrov (1974) and Molnar (1983) when describing deformation related to earthquakes by the Moment Tensor Summation method (MTS). Marrett and Allmendinger (1990) used the MTS approach and the tensor notation of Reches in the kinematic analysis of fault-slip data by first calculating the geometric moment and axes of extension and shortening for each measured fault, and then finding directional maxima of the shortening and extension axes for the complete fault array by applying Bingham distribution statistics. Kinematic analysis of fault-slip data was further improved by Cladouhos and Allmendinger (1993), who developed the FSFS method (Finite Strain from Fault-Slip data) for calculating the finite strain and the finite rotation of the deformed region. For analyzing cumulative deformation in highly faulted regions the finite strain approach of the FSFS method is probably better suited than the MTS method, which assumes infinitesimal strain. The FSFS method can also be used to reconstruct faulting-related block rotations in regions affected by domino-style faulting (Cladouhos and Allmendinger, 1993).

Most quantitative kinematic methods listed above (method of Reches (1978, 1983), the MTS and FSFS methods) require weighting of the fault-slip data with displacement, fault-surface area, and average distance between faults of the same size range (Reches, 1978, 1983; Marrett and Allmendinger, 1990). However, collecting these data often presents practical problems for field-based studies and is sometimes even impossible, especially when faults are poorly exposed. The only method avoiding this problem is the method of Marrett and Allmendinger (1990), which is equivalent to the MTS method with uniform weighting of the data.

In this article we describe the Multiple-slip method, which is an extension of the method of Reches (1978, 1983), MTS method (Kostrov, 1974; Molnar, 1983), and the kinematic analysis of Marrett and Allmendinger (1990). Our main goal is to derive an alternative way of calculating the weighting factors in the traditional infinitesimal approach of the moment tensor summation. We show that

* Corresponding author. Tel.: +386 40 795572.
E-mail address: jure.zalohar@guest.arnes.si (J. Žalohar).

0191-8141/$ – see front matter © 2008 Elsevier Ltd. All rights reserved.
doi:10.1016/j.jsg.2008.09.004

weighting of the fault-slip data can be performed based on (1) the number of parallel faults of the same size range, (2) their orientation, and (3) direction of slip along them. It is advantageous to use such approach, because the data needed by the Multiple-slip method can be obtained relatively easily, even when faults are poorly exposed. In the Multiple-slip method, the calculation of the weighting factors is based on the theory of Linear Elastic Fracture Mechanics (LEFM) and on the scaling properties of fracture and fault systems (see Table 1). We show that the values of weighting factors are also affected by the state of stress along the fault at the time of faulting. For natural fault systems, usually the only way to estimate the stress state that (re)activated the faults is the paleostress analysis (e.g., Carey and Brunier, 1974; Angelier, 1979, 1984, 1989, 1994; Fry, 1992, 1999, 2001). Our Multiple-slip method therefore combines kinematic analysis with the Gauss paleostress method (Žalohar and Vrabec, 2007). The Multiple-slip analysis is practically implemented in the T-TECTO 2.0 computer program (available on the following website: http://www2.arnes.si/~jzaloh/t-tecto_homepage.htm) and was thoroughly tested on many artificial and natural fault systems.

2. Scaling of the fault systems

Numerous studies at various scales and in different tectonic settings (see Bonnet et al., 2001, for a detailed overview) have shown that the size distribution of many fracture and fault systems follows a power-law (e.g., Marrett and Allmendinger, 1990; Bour and Davy, 1997, 1999; Main et al., 1999a,b, 2000; Main 2000a,b; Berkowitz et al., 2000):

$$N = \frac{A}{M^B} \rightarrow n(M) = \left|\frac{dN}{dM}\right| = B\frac{A}{M^{B+1}} \quad (1)$$

where M is the geometric moment, A is a parameter related to fault density, B is a distribution parameter, and N is a number of faults with geometric moment smaller or equal to M. The geometric moment M of a given fault is defined by the relationship $M = Su$, where S is the fault surface area and u is the amount of displacement along the fault. Equation (1) is derived from the Gutenberg–Richter law, which relates the earthquake magnitude m to the number of earthquakes in a specified amount of time, and was shown to be valid both in the regional and global scale (e.g., Main, 1996, 2000a,b; Main et al., 1999a,b, 2000; Udias, 1999; Turcotte, 2001; Bonnet et al., 2001; Al-Kindy and Main, 2003; Rundle et al., 2003). The value of the parameter B varies from region to region and does not necessarily remain constant during the seismic cycle or as strain localizes, but several studies nevertheless suggest that the global value of this parameter is approximately 2/3 (e.g., Kagan, 1997, 1999; Main and Al-Kindy, 2002; Al-Kindy and Main, 2003).

In nature, power-laws are valid only over a certain range of scales, limited by the upper M_{max} and the lower M_{min} boundary (e.g., Main, 1996, 2000a,b; Main et al., 1999a,b, 2000; Turcotte, 2001; Bonnet et al., 2001; Main and Al-Kyndi, 2002; Al-Kindy and Main, 2003). Intrinsic scale limit at the lower boundary may be due to atomic bonds or grain sizes, depending on the nature of the deforming materials (Bonnet et al., 2001). The upper limit has been more extensively studied; here finite thickness of the crust or sedimentary beds has been found to affect and violate simple scaling-law behavior in distribution of fractures and earthquakes (e.g., Davy, 1993; Volant and Grasso, 1994; Udias, 1999; Bonnet et al., 2001). In this way, the number of faults with geometric moment between M_1 and M_2 is:

$$N(M_1 < M < M_2) = \left|\int_{M_1}^{M_2} n(M)dM\right| = A\left[\frac{1}{M_1^B} - \frac{1}{M_2^B}\right] \quad (2)$$

and the total number of faults can be estimated as:

$$N_T = A\left[\frac{1}{M_{min}^B} - \frac{1}{M_{max}^B}\right] \approx \frac{A}{M_{min}^B} \quad (3)$$

Similarly, we can calculate the total geometric moment:

$$M_T = \left|\int_{M_{min}}^{M_{max}} Mn(M)dM\right| \approx \left|\int_0^{M_{max}} Mn(M)dM\right| = \frac{AB}{1-B}M_{max}^{1-B} \quad (4)$$

There are three unknown parameters in these equations, A, B and M_{max}. However, the number of the unknown parameters can be reduced to one (e.g., Scholz and Cowie, 1990; Marrett and Allmendinger, 1991), since for the largest fault the following relations hold:

$$\log N = \log 1 = 0 \text{ and } 0 = \log A - B\log M_{max} \quad (5)$$

therefore:

$$A = M_{max}^B \quad (6)$$

The total geometric moment is then:

$$M_T = \frac{B}{1-B}M_{max} \quad (7)$$

and from Equation (3) we obtain

Table 1
Explanation of the important quantities used in the text

Symbol	Explanation
N	Number of faults with geometric moment smaller or equal to M
A	Parameter related to the density of the faults
M	Geometric moment of the fault
M_S	Seismic moment of the earthquake
S	Fault surface area
u	Average displacement along the fault
B	Parameter related to the size-distribution of the faults
M_1 and S_1	Geometric moment and surface area of the smallest analyzed fault
M_2 and S_2	Geometric moment and surface area of the largest analyzed fault
M_T or M^T	Total geometric moment of a fault system
$\Delta\sigma$	Driving stress along the fault
c	Geometric constant of the fault; depends on the geometry of the model of the fault (circular fault, elliptical fault, etc.)
$\vec{\tau}$	Shear stress along the fault
$\vec{s}$	Slip direction along the fault
$\tau^{(r)}$	Resolved remote shear stress component in the direction of movement along the fault
σ_r	Residual frictional strength of the fault
μ	Coefficient of residual friction for sliding on a (re)activated pre-existing fault
$\overline{\sigma}_n$	Average normal stress on the fault
$\dot{\mathbf{u}} = \dot{u}_{ij}$	Strain rate
$\mathbf{u} = u_{ij}$	Displacement gradient tensor
$\mathbf{u}^{(S)}$	Symmetric part of the displacement gradient tensor, describing the true deformation of the medium (the strain tensor)
$\mathbf{W}$	Antisymmetric part of the displacement gradient tensor (the rotation tensor)
$\vec{\lambda}_1$, $\vec{\lambda}_2$ and $\vec{\lambda}_3$	Eigenvectors of the strain tensor $\mathbf{u}^{(S)}$
λ_1, λ_2 and λ_3	Eigenvalues of the strain tensor $\mathbf{u}^{(S)}$
$\vec{\phi}$	Axis of rotation, the axial vector of the rotation tensor $\mathbf{W}$
w_i	Weighting factor in the Multiple-slip method
Rm	Rotation parameter in the Multiple-slip method
Φ	Parameter describing the shape of the stress ellipsoid
D	Parameter describing the shape of the strain ellipsoid
ϕ_2	Angle of residual friction for sliding on (re)activated pre-existing faults

When the symbols are used to characterize individual faults or fault-sets, index i or k is added, for example, N_k, A_k, etc.

$$M_{\max} = (N^T)^{1/B} M_{\min} \tag{8}$$

Because the value of the parameter B is known to be approximately 2/3, the only unknown parameter in this equation is the geometric moment of the largest fault, $M_{\max}$. However, Equation (7) is only valid when the distribution of the faults follows Equation (1), ideally over the complete range of possible fault sizes from $M_{\min}$ to $M_{\max}$. It is known that for the largest faults/earthquakes the distributions observed in nature are not completely consistent with Equation (1) (e.g., Udias, 1999; Main, 2000b). If this is the case, Equation (7) can be used only as an approximation, which, however, depends on the case analyzed.

3. The driving stress

In natural fault systems the amount of slip u along the fault is related to the size of the fault (e.g., Clark and Cox, 1996; Marrett, 1996; Cladouhos and Marrett, 1996; Udias, 1999; Bonnet et al., 2001):

$$u \sim l^{\beta} \tag{9}$$

where β is a constant, and l is the fault length. A number of values for β was proposed in the literature, ranging from 0.5 to 2 (Bonnet et al., 2001). However, experimental and field-based studies demonstrated that its real value is close to 1 (e.g., Cowie and Scholz, 1992a; Bonnet et al., 2001). This is also in agreement with seismological studies (see Udias, 1999, for detailed discussion) and simple theoretical models of LEFM (Schultz and Fossen 2002; Gudmundsson, 2004; Xu et al., 2006). For a simple and planar fault-geometry, and for faults in an infinite medium (finite thickness of the crust or sedimentary beds may affect faulting) the LEFM suggests a linear dependence of the amount of slip on the fault size and the stress state along it:

$$u = c \cdot \Delta\sigma \sqrt{S} \tag{10}$$

which is also the form adopted in seismology (Udias, 1999). In the same manner we rewrite the equation for geometric moment (Udias, 1999):

$$M = Su = c \cdot \Delta\sigma S^{3/2} \tag{11}$$

Here $l \sim \sqrt{S}$ represents the size of the fault, c is a parameter accounting for the elastic properties of rock and the fault geometry, and $\Delta\sigma$ is the driving stress. For faults, the driving stress is defined as the resolved remote shear stress component in the direction of movement $\tau^{(r)} = \vec{\tau} \cdot \vec{s}$ minus the residual frictional strength of the surface σ_r (e.g., Jaeger and Cook, 1969; Cowie and Scholz, 1992b; Cooke, 1997; Forest et al., 1997; Schultz and Fossen, 2002):

$$\Delta\sigma = \mathrm{Max}\left(0, \left(\tau^{(r)} - \sigma_r\right)\right) \tag{12}$$

The residual frictional strength of faults is estimated as $\mu\bar{\sigma}_n$, where μ is the coefficient of residual friction for sliding on a (re)activated pre-existing fault, and $\bar{\sigma}_n$ is the average normal stress during faulting (e.g., Jaeger and Cook, 1969; Reches, 1978; Angelier, 1989; Ranalli and Yin, 1990; Reches et al., 1992; Yin and Ranalli, 1992, 1995; Udias, 1999; Ranalli, 2000; Fry, 2001). Equation (12) also assumes that only the faults on which the shear stress exceeds the frictional strength can be active. Note that for a given outcrop the same value of the coefficient of friction is used for all faults found in the same rock type. We assume that the frictional shear strength of faults depends on the type of the rock and not on the fault orientation.

It is also important to note that in the case of seismic slip along the fault the concept of the driving stress is equivalent to the concept of the stress drop during rupture. This way, the resolved remote shear stress component in the direction of movement $\tau^{(r)}$ can be taken as an approximation of the stress-state on the fault before failure, and the residual frictional strength σ_r of the fault can be taken as representing the residual stress-state after failure, on the assumption that the average normal stress does not change considerably during the rupture (Udias, 1999).

When deformation is aseismic, the difference between the resolved remote shear stress component in the direction of movement $\tau^{(r)}$ and the residual frictional strength σ_r causes aseismic elastoplastic and/or cataclastic flow of rocks, where most of deformation is accommodated by aseismic movements along the multiple fractures, dislocations and faults (e.g., Forest et al., 1997; Twiss and Unruh, 1998). From the theory of plastic deformations and frictional flow of rocks follows that the stress state is independent of the strain rate, but depends on the viscous properties of the deforming material (e.g., Forest et al., 1997; Dartevelle, 2003). This means that the stress does not change rapidly during the progressive elastoplastic/cataclastic deformation when the faults grow and the fault system develops (e.g., Jaeger and Cook, 1969; Dartevelle, 2003).

4. The multiple-slip mechanism

The calculation of incremental strain due to faulting in a region has been solved by Kostrov (1974) and Molnar (1983) in seismological studies of earthquakes, using seismic moment tensor summation:

$$\dot{\mathbf{u}} = \dot{u}_{ij} = \frac{1}{2GTV} \sum_{k=1}^{N} M_S^{(k)} m_{ij}^{(k)} \tag{13}$$

where $\dot{\mathbf{u}} = \dot{u}_{ij}$ is the total faulting-related strain rate, G is the shear modulus, V is the volume of the deforming medium, T is the time period of the earthquake record, and $M_S^{(k)}$ and $m_{ij}^{(k)}$ are the seismic moment and the moment tensor belonging to the k–th fault/earthquake, respectively (Reches, 1978, 1983; Marrett and Allmendinger, 1990; Kreemer et al., 2000). The seismic moment is defined as $M_S = GM$, where M is the geometric moment. The moment tensor m_{ij} is defined as the tensor product between the unit vector $S_{\min}$ defining the slip direction along the fault, and the unit normal vector to the fault plane, $\vec{n}$:

$$\mathbf{m} = m_{ij} = \vec{s} \otimes \vec{n} \tag{14}$$

The moment tensor is asymmetric because of the rotation inherent to simple shear deformation resulting from the fault slip (Marrett and Allmendinger, 1990).

The deformation due to the slip on a set of subparallel faults with subparallel direction of movement is then (Marrett and Allmendinger, 1990):

$$\mathbf{u}_k = \frac{M_k^T}{V} \mathbf{m}_k = \frac{M_k^T}{V} (\vec{s}_k \otimes \vec{n}_k) \tag{15}$$

where k denotes the index of the fault-set, and M_k^T is the total geometric moment of this k–th fault-set. We use the term "*fault-set*" for a group of subparallel faults with subparallel direction of motion, and the term "*fault system*" for a group of fault-sets with different orientations. The total displacement gradient tensor due to the movement along the faults belonging to all the fault-sets in the fault system is calculated by summing (e.g., Reches 1978, 1983):

$$\mathbf{u} = \sum_k \frac{M_k^T}{V} \mathbf{m}_k = \sum_k \frac{M_k^T}{V} (\vec{s}_k \otimes \vec{n}_k) \tag{16}$$

Assuming that strain is small, **u** can be decomposed into symmetric and antisymmetric parts, yielding the incremental strain and rotation tensors, $\mathbf{u}^{(S)}$ and **W** (Marrett and Allmendinger, 1990):

$$\mathbf{u}^{(S)} = \frac{1}{2}(u_{ij} + u_{ji}) \tag{17}$$

and

$$\mathbf{W} = \frac{1}{2}(u_{ij} - u_{ji}) \tag{18}$$

The eigenvectors $\vec{\lambda}_1$, $\vec{\lambda}_2$ and $\vec{\lambda}_3$ of the strain tensor $\mathbf{u}^{(S)}$ give the orientation of the principal incremental strain axes (kinematic axes), and the eigenvalues λ_1, λ_2 and λ_3 give their magnitudes. We use the sign convention from the theory of rock mechanics and paleostress analysis (e.g., Jaeger and Cook, 1969; Reches, 1978, 1983; Angelier, 1994), with positive eigenvalues representing shortening and compression, and negative eigenvalues representing extension and tension. We also choose that $\lambda_1 \geq \lambda_2 \geq \lambda_3$. Because the volume of the faulted rock does not change considerably during deformation, the trace of the strain tensor, $\mathrm{Tr}(\mathbf{u}^{(S)})$, approximately equals 0 (Reches, 1978, 1983):

$$\frac{\delta V}{V} = \lambda_1 + \lambda_2 + \lambda_3 = \mathrm{Tr}\left(\mathbf{u}^{(S)}\right) = 0 \tag{19}$$

Additionally, because the faulted rock volume always undergoes shortening in at least one direction, extension always appears in at least one other principal direction (e.g., Reches, 1978, 1983). The physical meaning of eigenvectors is therefore as follows: (1) vector $\vec{\lambda}_1$ represents the direction of greatest shortening, (2) vector $\vec{\lambda}_3$ represents the direction of greatest extension, and (3) vector $\vec{\lambda}_2$ can represent shortening or extension, varying from case to case.

The rotation tensor **W** describes rotation of material lines during deformation towards orientation parallel to the principal stretching axes (Cladouhos and Allmendinger, 1993). The amount and direction of rotation are defined by the axial vector $\vec{\phi}$ (Forest et al., 1997):

$$\vec{\phi} = -\frac{1}{2}\varepsilon\mathbf{W} \tag{20}$$

where

$$\varepsilon = \varepsilon_{ijk} = \frac{1}{2}(i-j)(j-k)(k-i)$$

represents a third-order permutation tensor. It is important to be aware that the rotation tensor **W** does not represent the rotation of rigid blocks between the faults (Cladouhos and Allmendinger, 1993), which can be measured by paleomagnetic or other methods. When a faulted region is viewed as a continuum, only the rotation of material lines is recognized, whereas the actual segments of the material between the faults do not necessarily rotate (Marrett and Allmendinger, 1990; Cladouhos and Allmendinger, 1993).

5. The Multiple-slip method

From Equation (16) follows that the strain and rotation tensors $\mathbf{u}^{(S)}$ and **W** can be calculated from:

$$\begin{aligned} \mathbf{u}^{(S)} &= \left[\sum_k \frac{M_k^T}{V}\mathbf{m}_k\right]^{(S)} = \left[\sum_k \frac{M_k^T}{V}\vec{s}_k \otimes \vec{n}_k\right]^{(S)}, \\ \mathbf{W} &= \left[\sum_k \frac{M_k^T}{V}\vec{s}_k \otimes \vec{n}_k\right]^{(A)} \end{aligned} \tag{21}$$

where k represents the index of the fault-set. The above equations may only be used for *homogeneous fault systems*, which consist of faults that were active at the same time in the same homogeneous stress and strain fields. However, natural fault systems are often *heterogeneous* as they typically comprise several homogeneous subgroups of faults, belonging to two or more deformation phases (e.g., Angelier, 1989; Nemcok and Lisle, 1995; Nemcok et al., 1999). The fault system heterogeneity can furthermore be a consequence of spatial and temporal variations of the stress and strain fields, such as those present during rupture or successive ruptures, or at the tip of a large fault. Because in general each homogeneous subsystem accommodated unique deformation boundary conditions, the deformation tensor calculated by applying Equations (21) to the entire heterogeneous fault system would have no physical meaning. Heterogeneous fault systems should therefore be separated into homogeneous subsystems prior to kinematic analysis. Additionally, fault slips affected by local stress and strain field perturbations should also be eliminated. The separation and filtering of fault-slip data can be effectively performed with the Gauss paleostress method (Žalohar and Vrabec, 2007) or some other paleostress technique for analyzing heterogeneous fault systems (e.g., Angelier, 1979, 1984; Etchecopar et al., 1981; Armijo et al., 1982; Nemcok and Lisle, 1995; Nemcok et al., 1999; Yamaji, 2000a,b, 2003; Yamaji et al., 2006).

The above Equations (21) will now be further simplified in the way they are used in the Multiple-slip method. First, it is important to realize that a natural homogeneous fault system can consist of several fault-sets, and that the faults of each fault-set can follow a different fault-size distribution. If we suppose that the distribution of faults belonging to a single fault-set can be approximated by the power-law distribution $N_k = A_k/M^{B_k}$, the complete distribution of all faults in the entire homogeneous system is $N = \sum_k A_k/M^{B_k}$. This distribution follows the power-law distribution with the exponent $B = 2/3$ only when B_k equals B for all included fault-sets. From the global validity of the power-law distribution with exponent $B = 2/3$ (e.g., Kagan, 1997, 1999; Main and Al-Kindy, 2002; Al-Kyndi and Main, 2003) we assume that in mature fault systems the fault-size distributions of all constituent fault-sets do indeed follow the power law distribution with $B_k = B = 2/3$.

In the next step, we assume that the total geometric moment for each fault-set is $M_k^T = A_k B_k M_{\mathrm{max},k}^{1-B}/(1-B_k)$ (Equation (4)). Solving this equation requires that the values of fault density parameter A_k, maximum geometric moment $M_{\mathrm{max},k}$ and distribution parameter B_k are known prior to analysis. We showed that the acceptable value of the parameter B_k is presumed to be 2/3. The other two parameters can be determined by careful field measurements of fault-scaling relationships and fault-size distribution. We may additionally suppose that for each fault-set $A_k = M_{\mathrm{max},k}^B$ (Equation (6)) and $M_{\mathrm{max},k} = (N_k^T)^{1/B} M_{\min}$ (Equation (8)), which in the best scenario leaves only the $M_{\mathrm{max},k}$ to be determined. However, the accurate estimation of $M_{\mathrm{max},k}$ or/and A_k represents a difficult task for field-based studies and is not always possible, especially when the faults are poorly exposed. Therefore, the Multiple-slip method adopts a different approach. The fault-slip data in many field-based studies are collected at small outcrops, where just a portion of each fault plane is visible. In the paleostress analysis the information on orientation of faults and slip direction along them is enough to make the calculation of paleostress tensor possible. It is advantageous to use this approach also in the Multiple-slip method, which then needs only one additional piece of information, and that is the number of parallel faults of specified size belonging to each fault-set.

To find the dependence of the weighting factors used in the moment tensor summation on the number of faults belonging to different fault-sets, we will now consider the following relations. First, the displacement gradient tensor for each fault-set becomes:

$$\mathbf{u}_k = \frac{M_k^T}{V}\mathbf{m}_k = \frac{BM_{max,k}}{(1-B)V}\mathbf{m}_k = \frac{BM_{min}}{(1-B)V}\left(N_k^T\right)^{1/B}\mathbf{m}_k \tag{22}$$

because $M_{\max,k} = (N_k^T)^{1/B}M_{\min}$ (Equation (8)). If we take into consideration that $M_{\min} = c\Delta\sigma_k S_{\min}^{3/2}$ (Equation (11)), we may also write:

$$\mathbf{u}_k = \frac{Bc\Delta\sigma_k S_{\min}^{3/2}}{(1-B)V}\left(N_k^T\right)^{1/B}\mathbf{m}_k = \frac{BcS_{\min}^{3/2}}{(1-B)V}\sum_{i=1}^{N_k^T}\Delta\sigma_i\frac{\left(N_k^T\right)^{1/B}}{N_k^T}\mathbf{m}_i \tag{23}$$

where index i denotes the i–th fault. The driving stress $\Delta\sigma_i$ along the i–th fault is supposed to be equal for all faults of the k–th fault-set, so $\Delta\sigma_i = \Delta\sigma_k$. We also take into account that the minimum fault surface area, $S_{\min}$, is believed to be equal for all fault-sets, because it is constrained by the scale of atomic bonds or grain sizes (e.g., Bonnet et al., 2001). The total displacement gradient tensor corresponding to slip on faults from all fault-sets that comprise the homogeneous system can be calculated by summing:

$$\begin{aligned}\mathbf{u} &= \sum_k\left[\frac{BcS_{\min}^{3/2}}{(1-B)V}\Delta\sigma_k\left(N_k^T\right)^{1/B}\mathbf{m}_k\right]\\ &= \frac{BcS_{\min}^{3/2}}{(1-B)V}\sum_k\left[\Delta\sigma_k\left(N_k^T\right)^{1/B}\mathbf{m}_k\right]\end{aligned} \tag{24}$$

presuming that the parameters B, c, S_{min} and V have the same value for all fault-sets. In order to calculate the total displacement gradient tensor $\mathbf{u}$, we should therefore know: (1) the orientation of each fault and direction of slip along it (this constrain the moment tensor $\mathbf{m}_i$), (2) the total number of faults belonging to each fault-set N_k^T, and (3) the driving stress on each fault $\Delta\sigma_i = (\tau^{(r)} - \mu\bar{\sigma}_n)_i$. Usually the total number of faults N_k^T cannot be measured directly, but can be estimated from the number of faults N_k of the size ranging between S_1 and S_2. From Equations (2), (6) and (8) we derive:

$$\begin{aligned}N_k &= \frac{(c\Delta\sigma_k)^B S_{\min}^{3B/2}N_k^T}{(c\Delta\sigma_k)^B}\left(\frac{1}{S_1^{3B/2}} - \frac{1}{S_2^{3B/2}}\right)\\ &= N_k^T\left(\frac{1}{S_1^{3B/2}} - \frac{1}{S_2^{3B/2}}\right)S_{\min}^{3B/2}\end{aligned} \tag{25}$$

So, N_k^T equals:

$$N_k^T = \frac{N_k}{\left(\frac{1}{S_1^{3B/2}} - \frac{1}{S_2^{3B/2}}\right)S_{\min}^{3B/2}} = N_k K \tag{26}$$

with $K = 1/[(S_1^{-3B/2} - S_2^{-3B/2})S_{\min}^{3B/2}]$. In this way Equation (24) can be rewritten in terms of N_k rather than N_k^T:

$$\mathbf{u} = \frac{BcS_{\min}^{3/2}K^{1/B}}{(1-B)V}\sum_k\Delta\sigma_k(N_k)^{1/B}\mathbf{m}_k \tag{27}$$

The next question is how to calculate the driving stress. In fault-slip studies the stress state at the time of faulting can be reconstructed from the paleostress analysis. The driving stress $\Delta\sigma_i$ can then be calculated from the reconstructed paleostress tensor. Therefore, the Multiple-slip method should start with the paleostress procedure using the Gauss paleostress method (Žalohar and Vrabec, 2007), followed by the moment tensor summation. The advantage of the Gauss method over other paleostress determination techniques is that it enables determining the optimal coefficient of friction μ for sliding on the (re)activated pre-existing faults, which is required for calculating the driving stress in the Multiple-slip method. With the analysis of the Mohr diagrams the Gauss method also determines the stress tensor of the form $\boldsymbol{\sigma} = const.\boldsymbol{\sigma}^{true}$, where $\boldsymbol{\sigma}^{true}$ represents the true stress state at the time of faulting, and *const.* is some unknown constant. This allows the determination of the ratio of the principal stress magnitudes. The actual magnitudes of the stress tensor components can also be calculated, but only when newly formed conjugate fault sets are present and the strength properties of rocks (failure envelope) at the time of faulting are known (see Angelier, 1989, for detailed discussion). These conditions are not met in most cases, and the full stress tensor thus cannot be calculated. The tensor $\boldsymbol{\sigma} = konst.\boldsymbol{\sigma}^{true}$ is used instead, since in this case only the coefficient of friction for sliding along the (re)activated pre-existing faults needs to be known (e.g., Angelier, 1989; Žalohar and Vrabec, 2007). This tensor is used for calculating the shear and normal stress components along each fault, which, however, allows only the calculation of the ratio $\Delta\sigma_1 : \Delta\sigma_2 : \Delta\sigma_3 \ldots$ between the values of the driving stresses acting on the faults. This means that the displacement gradient tensor $\mathbf{u}$ calculated by the Multiple-slip method will also be of the form $\mathbf{u} = const.\mathbf{u}^{true}$. Under these constraints it is possible to calculate: (1) the direction of kinematic axes, (2) the ratio between principal strains, and (3) the direction and relative magnitude of rotation, while the actual magnitudes of deformation and rotation remain unknown.

Taking into consideration the above discussion, the problematic factors $BcS_{\min}^{3/2}K^{1/B}/(1-B)V$ in Equation (27) have to be neglected. Using Equation (12) and simplified Equation (27), it follows that the displacement gradient tensor linearly depends on the number of faults having sizes between S_1 and S_2:

$$\begin{aligned}\mathbf{u} &\sim \sum_k\Delta\sigma_k(N_k)^{1/B}\mathbf{m}_k\\ &= \sum_k\left[\sum_{i=1}^{N_k}\mathrm{Max}\left(0,(\tau^{(r)} - \mu\bar{\sigma}_n)\right)_i\frac{(N_k)^{1/B}}{N_k}\mathbf{m}_i\right]\\ &= \sum_i w_i\mathbf{m}_i\end{aligned} \tag{28}$$

where the weighting factors are defined as $w_i = (N_i^{1/B}/N_i)\cdot\mathrm{Max}(0,(\tau^{(r)} - \mu\bar{\sigma}_n))_i$. The appropriate value of $N_i = N_k$ should be known for each fault and/or fault-set. The weighting factors w_i can be calculated from the resolved driving stress and the number of faults, N_k, with specified size belonging to different fault-sets. Generally, the total number of faults, N_k, with the size ranging between S_1 and S_2 in the volume V cannot be measured directly, because the fault system might not be completely exposed. N_k should be estimated from measurements of the average fault density (defined as a number of faults of specified size per volume V) at several outcrops. The average density $\bar{n}$ can be calculated as the average of the density measurements from several outcrops located in as wide an area as possible. If V' is the total volume of exposed rocks in all observed outcrops, and V is the total volume containing the complete fault system, the number of faults N_k can be roughly estimated as $N_k \approx \bar{n}(V/V')$. It is important to note that the faulting related deformation is not homogeneous in the case of spatially varying fault density of fractal fault systems (Bonnet et al., 2001). Therefore, performing the Multiple-slip method for faults observed at individual outcrops should be interpreted as a rough approximation of the local strain field. In contrast, performing the Multiple-slip method for combined measurements of faults in several outcrops should be interpreted as a rough approximation of the regional strain field accommodated by the complete fault system in the volume V. How rough is this approximation of the local or regional strain field, depends on the case analyzed, and this can be checked by the T-TECTO computer program. The program allows the user to manually change the values of the

B–parameter, the coefficient of friction μ, and the value of N_k for each fault-set. Varying these parameters indicates how the inaccuracy in sampling of the fault population (quantified by N_k and B) and the inaccuracy in calculation of the driving stress ratio $\Delta\sigma_1 : \Delta\sigma_2 : \Delta\sigma_3 \ldots$ would affect results of the kinematic analysis. Note that the driving stress depends on the coefficient of friction. If the results are numerically stable when varying N_k, B and μ for a reasonable amount, they can be treated as reliable. Otherwise, they should be interpreted with a great caution.

6. The rotation parameter

Because the Multiple-slip method generally does not provide the full displacement gradient tensor as only the relative values of its components are calculated, the total amount of rotation ϕ cannot be determined either. We can only calculate the direction of the axial vector $\vec{\phi}$ belonging to the rotation tensor **W**. Therefore, we define another measure for the relative amount of rotation, the rotation parameter *Rm*:

$$Rm = \frac{\left\|\mathbf{u}^{(9)}\right\| - \left\|\mathbf{u}^{(S),(9)}\right\|}{\left\|\mathbf{u}^{(9)}\right\|} \tag{29}$$

where

$$\begin{aligned} \left\|\mathbf{u}^{(9)}\right\| &= \|(u_{11}, u_{22}, u_{33}, u_{12}, u_{13}, u_{23}, u_{21}, u_{31}, u_{32})\|, \\ \left\|\mathbf{u}^{(S),(9)}\right\| &= \|(u_{11}, u_{22}, u_{33}, u_{12}, u_{13}, u_{23}, u_{12}, u_{13}, u_{23})\| \end{aligned} \tag{30}$$

The rotation parameter *Rm* represents a normalized measure of the relative magnitude of rotation. It is defined as the difference between the displacement gradient tensor and its symmetric part, which are represented by nine-dimensional vectors $\mathbf{u}^{(9)}$ and $\mathbf{u}^{(S),(9)}$ in the nine-dimensional parameter-space of the components of the displacement gradient tensor. The possible values of *Rm* range from 0, representing no rotations, to 1, representing the largest rotations.

7. Testing the Multiple-slip method

The efficiency and reliability of the Multiple-slip method is demonstrated on one natural and several artificial fault-slip datasets. The artificial datasets were generated by AmontonWin computer program, which is part of the T-TECTO suite. AmontonWin generates a prescribed number of faults which are either randomly orientated, or follow a pre-defined distribution of orientations. The direction of slip along the faults is set parallel to the resolved shear stress on the fault planes, calculated from the input stress tensor. In Test 1, the faults were generated under the stress state characterized by maximum compression in the N–S direction and minimum compression in the W–E direction, while the intermediate stress axis was vertical. The ratio between the principal stress magnitudes was set to 0.96: 0.26: 0.09, so the value of the parameter $\Phi = (\sigma_1 - \sigma_2)/(\sigma_1 - \sigma_3)$ was 0.2. In Test 2, the faults were generated in extensional stress state with maximum compression vertical. In Test 1 and Test 2 initial paleostress analysis is therefore not required since the stress tensors are known. Only for the Test 3, in which we analyze a natural fault system, the paleostress analysis was needed prior to the moment tensor summation in order to calculate the paleostress tensor. In the next step of the analysis of all three cases, the weighting factors w_i were calculated for all faults based on the resolved driving stress and the number of faults belonging to different fault-sets. Finally, the moment tensor summation was performed by using the weighted data.

7.1. Test 1

In Test 1 we investigated how the asymmetry of the fault system influences the calculated relative magnitude of rotation. We analyzed four artificial fault systems with faults in parallel, conjugate and random orientation, shown in Fig. 1.

7.1.1. Case 1

The most asymmetric fault system consists of only one fault-set (Fig. 1a). In this case the calculated axis of rotation is parallel to the intermediate kinematic axis $\vec{\lambda}_2$. The $\vec{\lambda}_1$ and $\vec{\lambda}_3$ axes, which represent the direction of the maximum shortening and extension, are horizontal and inclined at an angle of 45° with respect to the average strike of fault planes. The intermediate kinematic axis is vertical and lies on the fault planes. The maximum shortening and maximum extension have N–S and W–E directions, respectively. The calculated value of the parameter $D = (\lambda_1 - \lambda_2)/(\lambda_1 - \lambda_3)$ is 0.5. In addition, the Multiple-slip method indicates the CW sense of rotation around vertical axis (indicated by the symbol ⊗) with the rotation parameter *Rm* equal to 0.71.

7.1.2. Case 2

This example represents a more symmetric fault system (Fig. 1b) than Case 1. However, its two fault-sets do not consist of the same number of faults. The first fault-set consists of 20 NW–SE striking dextral strike-slip faults, while the second fault-set consists of only 10 NE–SW striking sinistral strike-slip faults. The calculated relative magnitude of rotation is smaller than in Case 1. If faults follow the power-law size-distribution with the B value of 2/3, the calculated rotation parameter *Rm* is equal to 0.44. The rotation has CW sense around vertical axis (indicated by the symbol ⊗). The calculated value of the parameter $D = (\lambda_1 - \lambda_2)/(\lambda_1 - \lambda_3)$ is 0.49.

7.1.3. Case 3

The case represents a fully symmetric conjugate fault system, where both fault-sets have the same number of faults (Fig. 1c). The calculated value of the rotation parameter *Rm* is 0.09. Theoretically, the rotation parameter should be equal to 0. However, the value obtained by the Multiple-slip method is different from 0 due to the angular dispersion of fault orientations, which was purposely introduced during the fault-generating stage in order to obtain more realistic data. The calculated value of the parameter $D = (\lambda_1 - \lambda_2)/(\lambda_1 - \lambda_3)$ is 0.49.

7.1.4. Case 4

The last case analyzed in Test 1 consists of 50 faults with random orientation. We expect the deformation accommodated by such fault system to be symmetrical, and the Multiple-slip method confirms this assumption. The calculated rotation parameter *Rm* is only 0.14, and the calculated value of the parameter $D = (\lambda_1 - \lambda_2)/(\lambda_1 - \lambda_3)$ is 0.31.

The results of Test 1 show that the relative magnitude of the rotation (quantified by the parameter *Rm*) is directly related to the asymmetry of the fault system. Highly asymmetric fault systems accommodate large rotations (high value of *Rm*), while symmetric fault systems can only be active in the non-rotational strain field (low value of *Rm*).

7.2. Test 2

In Test 2 we analyzed dependence of the calculated strain on the coefficient of residual friction. For this purpose we generated two fault-sets in extensional stress regime with maximum compression vertical (Fig. 2). The first fault-set consists of 20 south-dipping normal faults, and the second set consists of 20 NW–SE striking normal-dextral faults. The resolved stress depends on fault orientation and is not the same for the two fault sets (Fig. 2b). Because the weighting factors in the Multiple-slip method depend on the driving stress $\Delta\sigma_i = \tau^{(r)} - \mu\bar{\sigma}_n$, which has the friction coefficient $\mu = \tan\phi_2$ as

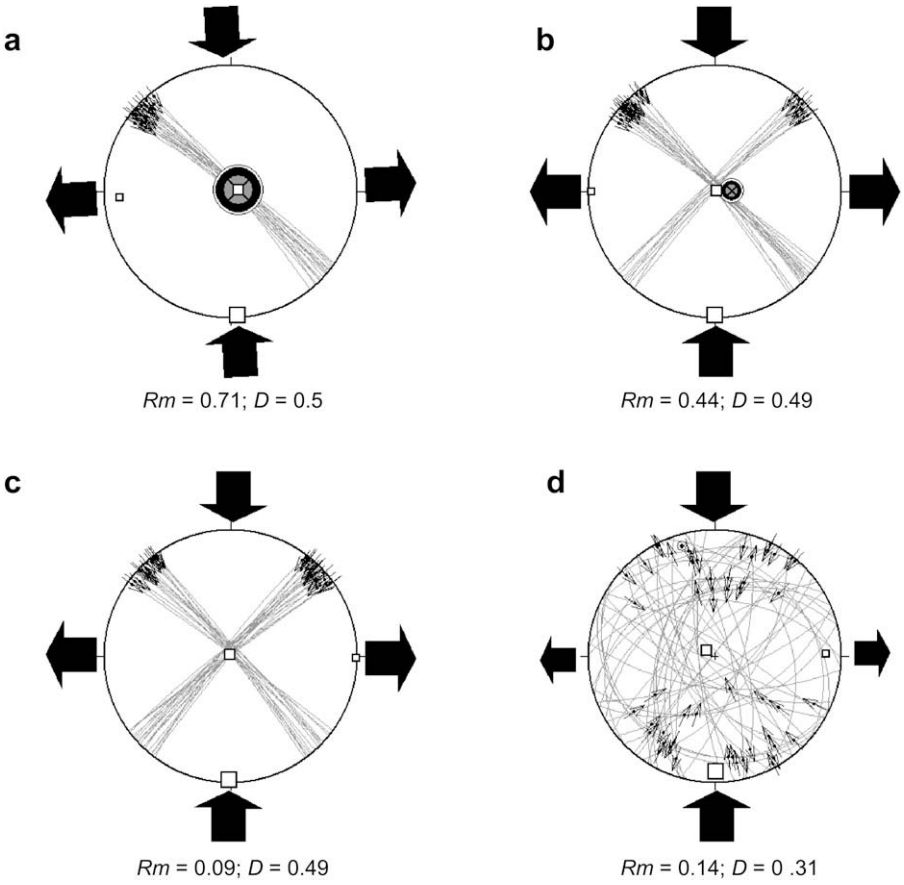

Fig. 1. An example illustrating the dependence of the calculated relative magnitude of rotation in the case of fault systems exhibiting different degree of asymmetry. The orientation of kinematic axes is indicated by large arrows, and the direction of rotation is indicated by the symbol ⊗. (a) In the case of a single fault-set the clockwise rotation is largest, and its relative magnitude is represented by the rotation parameter $Rm = 0.71$. (b) This case represents a conjugate fault-system with two perpendicular fault-sets. However, the fault system is not symmetrical, because the two fault-sets contain different numbers of faults. There are 20 NW–SE striking dextral strike-slip faults and 10 NE–SW striking sinistral strike-slip faults. The relative magnitude of rotation, quantified by the rotation parameter *Rm* equal to 0.44, is smaller than in Case (a). (c) This case represents ideally symmetric conjugate fault system consisting of two fault-sets with equal number of faults. The rotations are almost absent, which is indicated by the small value of the rotation parameter, $Rm = 0.09$. (d) The last case represents a symmetric fault system consisting of 50 randomly orientated faults. In this case the rotations are also almost absent, which is indicated by $Rm = 0.14$.

a parameter, the value of the friction coefficient will directly influence the results of the Multiple-slip method. This is demonstrated in Fig. 2c and d, where $\phi_2 = 0^0$ and $\phi_2 = 20^0$ were used, respectively. In both cases, the value of the parameter $D = (\lambda_1 - \lambda_2)/(\lambda_1 - \lambda_3)$ differs from that of $\Phi = (\sigma_1 - \sigma_2)/(\sigma_1 - \sigma_3)$, which is equal to 0.2. We obtain $D = 0.27$ in the first case and $D = 0.14$ in the second. Test 2 demonstrates importance of the frictional shear strength of faults on the estimation of the faulting-related deformation.

7.3. Test 3

In Test 3 we analyzed a natural fault system observed in the Cretaceous limestone of the Vremščica quarry in Slovenia (lon = 14,088°, lat = 45,679°), located in the Outer Dinarides fold-and-thrust belt. We measured the orientation and direction of slip along 42 faults (Fig. 3a) with fault surface area ranging from around 1 m^2 to 100 m^2, and the length of faults ranging from around 1 m to 10 m. First we performed paleostress analysis using the Gauss method. The Mohr diagram (Fig. 3b) gives the friction coefficient $\mu = \tan(35^0 \pm 5^0) = 0.7 \pm 0.15$. From the Mohr diagram it is evident that the inversion results are in agreement with the theory of fault-reactivation, since for all faults the resolved shear stress exceeds frictional strength, illustrated by a straight line $\tau = 0.7\sigma_n$ (Amonton's law). The calculated stress tensor shows that faults were active in a strike-slip stress regime with maximum horizontal compression in the NNW–SSE direction, and with the parameter $\Phi = (\sigma_1 - \sigma_2)/(\sigma_1 - \sigma_3)$ equal to 0.1 (Fig. 3a). This stress state is typical of the post-orogenic Pliocene-recent strike-slip deformation episode in the northern Dinarides (e.g., Vrabec and Fodor, 2006).

Paleostress calculation was followed by the Multiple-slip method, the results of which are shown in Fig. 3c and d. In the test shown in Fig. 3c the moment tensor summation was performed using unweighted data, whereas in the test shown in Fig. 3d the data were weighted with weighting factors $w = (N^{3/2}/N)(\tau^{(r)} - 0.7\sigma_n)$. Here N represents the number of faults belonging to the particular fault-set, while $\tau^{(r)}$ and σ_n are the resolved shear stress in the direction of movement and the normal stress, respectively. We defined three fault-sets with average orientation of faults 220/70, 180/40 and 270/80, comprising 9, 4 and 6 faults, respectively. All other faults have random orientation, therefore they were interpreted as belonging to a random fault array and were weighted with $w = 1 \cdot (\tau^{(r)} - 0.7\sigma_n)$.

Results of the Multiple-slip method show little variation between the two cases (Fig. 3c and 3d). Calculated kinematic axes are approximately parallel to the principal axes of the paleostress tensor, and value of the parameter $D = (\lambda_1 - \lambda_2)/(\lambda_1 - \lambda_3)$ is 0.44 in both cases. In the first case the direction of the rotation axis is 219/22, with $Rm = 0.28$, while in the second case the direction of the rotation axis is 245/5, with $Rm = 0.26$. In both cases the results indicate CW sense of rotation around a nearly horizontal axis.

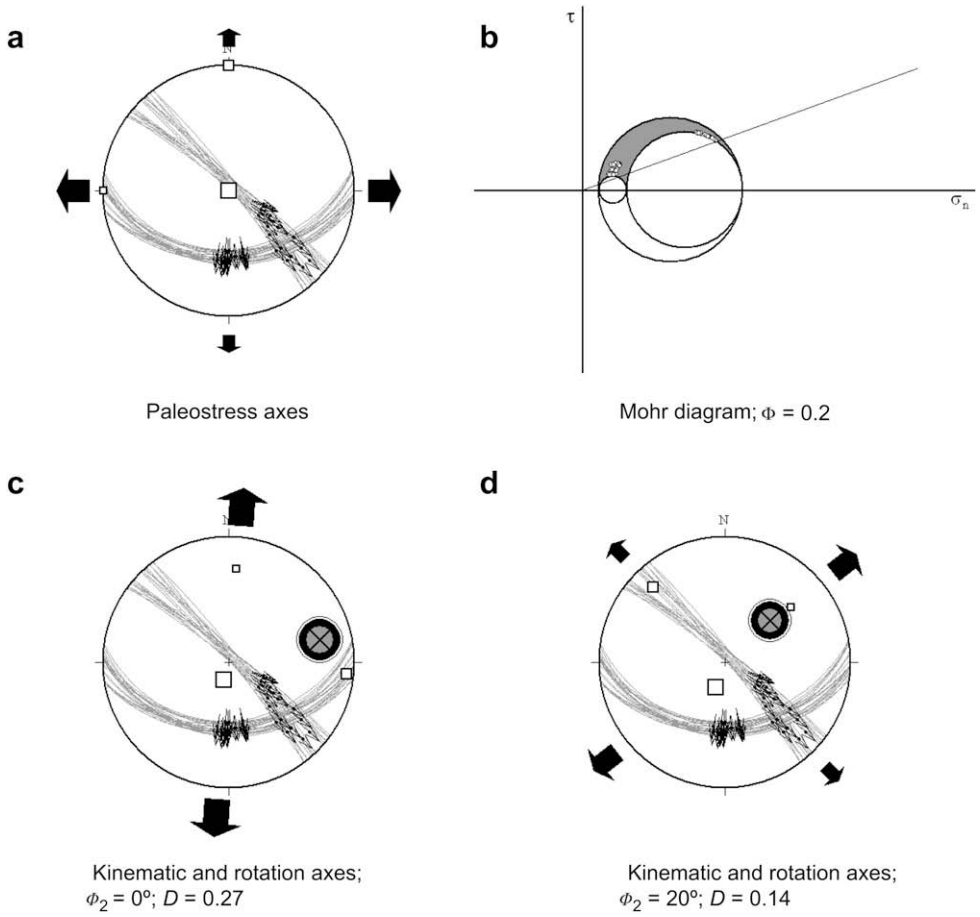

Fig. 2. An example illustrating the effect of the frictional shear strength of faults on the calculated direction of kinematic and rotation axes. (a) The fault system consists of two fault-sets compatible with extensional stress state with maximum compression vertical. (b) Mohr diagram illustrates the state of stress on the faults. σ_n is the normal stress and τ is the shear stress. (c) and (d) show the results of kinematic analysis obtained by the Multiple-slip method using two different values of the coefficient of friction $\mu = \tan \phi_2$. Here ϕ_2 represents the slope of the straight line illustrating the Amonton's law on the Mohr diagram shown in (b). Large arrows indicate shortening or extension. See text for details.

Test 3 demonstrates that the asymmetry of the fault system is related to the relative magnitude of the rotation accommodated by the faults, which was also shown in Test 1. The fault system analyzed in Test 3 is almost symmetrical, because it has accommodated nearly non-rotational deformations.

8. Discussion

The question whether stress (paleostress analysis) or strain (kinematic analysis) approach is better suited to fault-slip data treatment is a subject of much discussion (e.g., Marrett and Peacock, 1999; Nieto-Samaniego, 1999; Tikoff and Wojtal, 1999; Watterson, 1999; Pollard, 2000; Gapais et al., 2000). An useful insight into this problem can be found in the continuum theory of dislocations and in the theory of crystal plasticity (e.g., Forest et al., 1997, 2000), which are well-defined physical theories. The continuum theory of dislocations is a way to think of dislocation theory as a physical field theory (Forest et al., 1997). In this theory, yielding and hardening behavior of crystals mainly depends on the growth of dislocation population and on the development of dislocation structures inside the volume element V (Forest et al., 2000). Plastic deformation of crystals is related to activation of slip systems, which are defined by numerous small dislocations. Equations that describe the kinematics of the elastoplastic deformation must be constrained by flow rules and hardening laws. In several studies a formulation of viscoplasticity is adopted through the generalized Schmid law (Forest et al., 1997). Basic mathematical description (1) of the multi-mechanism plasticity of crystals and (2) of the moment tensor summation in the description of faulting-related deformation are quite similar. Within the framework of the moment tensor summation, faults are treated in the same way as dislocations or slip systems in the theory of crystal plasticity. It is also assumed that a dense fault array can be described as a continuum of dislocations. This further suggests that the fault strain could be related to stress through some similar relationship to that of the Schmid law in the theory of crystal plasticity. Indeed, a correspondence with the Schmid law can be found in the theory of LEFM with its concept of the driving stress. The only difference is that the driving stress does not account for the history of deformations, whereas the Schmid law does. Therefore, the results of the Multiple-slip method only describe the final stage of the deformation accommodated by the faults.

Because the driving stress is used in the Multiple-slip method, Equation (28) represents an explicit constitutive relationship between the stress and strain, where the strain tensor is directly related to the stress tensor and to the material internal structure, which is defined by spatial and orientational distribution of faults. If we assume that the deforming material is isotropic, the principal axes of the strain and stress tensors are parallel and proportional in the magnitudes, and the values of the parameters Φ and D are equal (e.g., Etchecopar et al., 1981; Twiss and Unruh, 1998; Tikoff and Wojtal, 1999). However, results of our numerical tests show that in the case of asymmetric fault systems, such as that analyzed in Test 2, a large inconsistency exists between the stress and strain, which indicates a more complex stress–strain relationship. The material

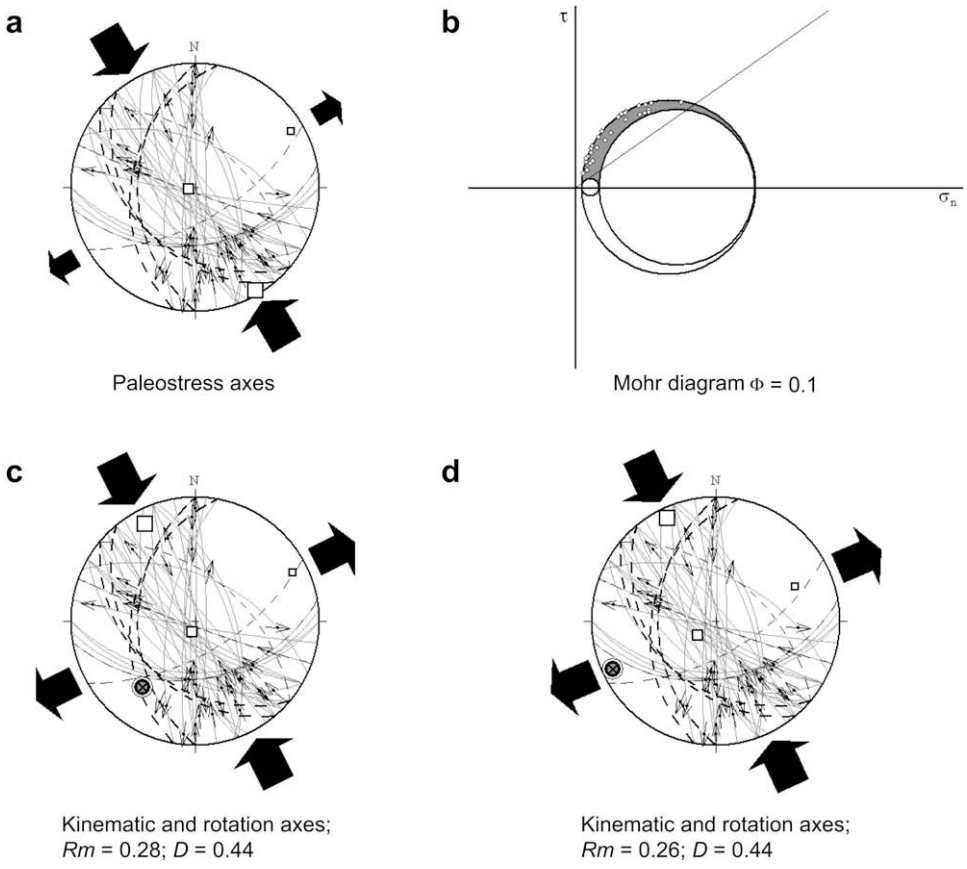

Fig. 3. Analysis of the natural fault system observed in the Vremščica quarry in Slovenia. The system consists of 42 faults compatible with strike-slip stress regime that has maximum horizontal compression in the NNW–SSE direction (a). Thick dashed lines show bedding orientation, while thin dashed lines show joint orientation. Mohr diagram (b) indicates that the coefficient of friction at the time of faulting was 0.7 ± 0.15. (c) and (d) show the results of the Multiple-slip method for unweighted data (c), and for weighted data (d). Large arrows indicate shortening or extension. See text for details.

behavior is therefore strongly dependent on its anisotropy, defined by the asymmetry of the fault system present within. In addition, different values of the parameters Φ and D obtained in Tests 1 and 3 also indicate complex and non-linear stress–strain relationship. In fact, in Tests 1 (a), (b) and (c) no relationship between the parameters Φ and D exists, because the deformation is two-dimensional with $\lambda_2 = 0$, $\lambda_1 = -\lambda_3$ and $D = 0.5$, in which case the intermediate principal stress and the parameter Φ have no effect on the slip direction along the faults (e.g., Jaeger and Cook, 1969).

The theory of the Multiple-slip method implies that a simple kinematic analysis is not always sufficient to correctly constrain the faulting-related strain. This suggests that the classical view of the kinematic analysis being independent from the paleostress analysis should be abandoned. In contrast to other known paleostress and kinematic techniques, the Multiple-slip method makes possible a combined stress–strain analysis of fault-slip data.

9. Conclusions

The Multiple-slip method is a simple and quick way for estimating principal characteristics of faulting-related strain. The aim of this method is (1) to calculate the direction of kinematic axes, which represent the direction of maximum shortening and extension, and (2) to estimate the direction and relative magnitude of faulting-related rotation. To apply the Multiple-slip method, three elements must be known for each fault: (1) the fault plane orientation, (2) the slip direction, and (3) the number of parallel faults in the same size range. Weighting factors in the Multiple-slip method depend on the number of faults in a particular fault-set and on the driving stress. The driving stress on each fault is calculated from the slip direction and the paleostress tensor, which represents the stress state at the time of faulting. Because the stress tensor is needed in the Multiple-slip method for the strain tensor calculation, the analysis also requires reconstruction of the paleostress state. In the Multiple-slip method, the calculated paleostress tensor should be of the form $\boldsymbol{\sigma} = const.\boldsymbol{\sigma}^{true}$, where $\boldsymbol{\sigma}^{true}$ represents the true stress state at the time of faulting, and $const.$ is some unknown constant. When analyzing natural fault-slip data, it is supposed that the actual magnitudes of the paleostress tensor are usually not known (e.g., Angelier, 1989, 1994). Consequently, the displacement gradient tensor calculated by the Multiple-slip method will also be of the form $\mathbf{u} = const.\mathbf{u}^{true}$. This means that kinematic analysis of the fault-slip data using the Multiple-slip method usually only allows estimation of (1) the direction of kinematic axes, (2) the ratio between the principal strains, and (3) the direction and relative magnitude of rotation. The relative magnitude of rotation is quantified by the rotation parameter *Rm*. Values of *Rm* close to 0 indicate a small amount of rotation, while values close to 1 indicate large rotation. This rotation does not represent the rotation of the blocks bounded by the faults, but it represents the rotation of material lines attached to the rock continuum.

The Multiple-slip method can be used to constrain the stress–strain relationship associated with faulting. Our tests of the method suggest that the stress–strain relationship depends on the frictional properties of faults and on the material anisotropy, which is controlled by the degree of asymmetry of the fault system.

Acknowledgements

The authors are grateful to Gerald Roberts for his careful review and many constructive comments. We also greatly appreciate the useful comments of an anonymous reviewer and the thorough editorial handling of Robert E. Holdsworth.

References

Al-Kindy, F.H., Main, I.G., 2003. Testing self-organized criticality in the crust using entropy: A regionalized study of the CMT global earthquake catalogue. Journal of Geophysical Research 108 (B11), 2521, doi:10.1029/2002JB002230.

Angelier, J., 1979. Determination of the mean principal directions of stress for a given fault population. Tectonophysics 56, T17–T26.

Angelier, J., 1984. Tectonic analysis of fault slip data sets. Journal of Geophysical Research 89, 5835–5848.

Angelier, J., 1989. From orientation to magnitudes in paleostress determinations using fault slip data. Journal of Structural Geology 11, 37–50.

Angelier, J., 1994. Paleostress determinations. In: Hancock, P.L. (Ed.), Continental Deformations. Pergamon Press, Tarrytown, NY, pp. 53–100.

Armijo, R., Carey, E., Cisternas, A., 1982. The inverse problem in microtectonics and the separation of tectonic phases. Tectonophysics 82, 145–160.

Berkowitz, B., Bour, O., Davy, P., Odling, N., 2000. Scaling of fracture connectivity in geological formations. Geophysical Research Letters 27, 2061–2064.

Bonnet, E., Bour, O., Odling, N.E., Davy, P., Main, I., Cowie, P., Berkowitz, B., 2001. Scaling of fracture systems in geological media. Reviews of Geophysics 39, 347–383.

Bour, O., Davy, P., 1997. Connectivity of random fault networks following a power-law fault length distribution. Water Resources Research 33, 1567–1583.

Bour, O., Davy, P., 1999. Clustering and size distributions of fault patterns: theory and measurements. Geophysical Research Letters 26, 2001–2004.

Carey, E., Brunier, B., 1974. Analyse théoretique et numérique d'un modèle mécanique élémentaire appliqué a l'étude d'une population de failles. Comptes Rendus de l'Académie des Sciences, Paris D279, 891–894.

Cladouhos, T.T., Allmendinger, R.W., 1993. Finite strain and rotation from fault slip data. Journal of Structural Geology 15, 771–784.

Cladouhos, T.T., Marrett, R., 1996. Are fault growth and linkage models consistent with power-law distributions of fault lengths? Journal of Structural Geology 18, 281–294.

Clark, R.M., Cox, S.J.D., 1996. A modern regression approach to determining fault displacement-length scaling relationships. Journal of Structural Geology 18, 147–154.

Cooke, M.L., 1997. Fracture localization along faults with spatially varying friction. Journal of Geophysical Research 102, 22425–22434.

Cowie, P.A., Scholz, C.H., 1992a. Displacement-length scaling relationship for faults: data synthesis and discussion. Journal of Structural Geology 14, 1149–1156.

Cowie, P.A., Scholz, C.H., 1992b. Physical explanation for the displacement-length relationship of faults using a post-yield fracture mechanics model. Journal of Structural Geology 14, 1133–1148.

Dartevelle, S., 2003. Numerical and Granulometric Approaches to Geophysical Granular Flows, Ph.D. thesis, Michigan Technological University, Michigan.

Davy, P., 1993. On the frequency-length distribution of the San Andreas fault system. Journal of Geophysical Research 98, 12.141–12.151.

Etchecopar, A., Vasseur, G., Daigniers, M., 1981. An inverse problem in microtectonics for the determination of stress tensors from fault striation analysis. Journal of Structural Geology 3, 51–65.

Forest, S., Cailletaud, G., Sievert, R., 1997. A Cosserat theory for elastoviscoplastic single crystals at finite deformation. Archives of Mechanics 49, 705–736.

Forest, S., Barbe, F., Cailletaud, G., 2000. Cosserat modelling of size effects in the mechanical behaviour of polycrystals and multi-phase materials. International Journal of Solids and Structures 37, 7105–7126.

Freund, R., 1970. The geometry of the faulting in the Galilee. Israel Journal of Earth Sciences 19, 117–140.

Fry, N., 1992. A robust approach to the calculation of paleostress fields from fault plane data: Discussion. Journal of Structural Geology 14, 635–637.

Fry, N., 1999. Striated faults: visual appreciation of their constraint on possible paleostress tensors. Journal of Structural Geology 21, 7–21.

Fry, N., 2001. Stress space: striated faults, deformation twins, and their constraints on paleostress. Journal of Structural Geology 23, 1–9.

Gapais, D., Cobbold, P.R., Bourgeois, O., Rouby, D., Urreiztieta, M., 2000. Tectonic significance of fault-slip data. Journal of Structural Geology 22, 881–888.

Gudmundsson, A., 2004. Effects of Young's modulus on fault displacement. C.R. Geoscience 336, 85–92.

Jaeger, J.C., Cook, N.G.W., 1969. Fundamentals of Rock Mechanics. Methuen, London, 515 pp.

Kagan, Y.Y., 1997. Seismic moment-frequency relation for shallow earthquakes: Regional comparison. Journal of Geophysical Research 102, 2835–2852.

Kagan, Y.Y., 1999. Universality of the seismic moment-frequency relation. Pure Applied Geophysics 155, 537–573.

Kostrov, V.V., 1974. Seismic moment and energy of earthquakes, and seismic flow of rocks. Izvestiya Academy of Sciences of the USSR (Physics of Solid Earth) 1, 23–40.

Kreemer, C., Haines, J., Holt, W.E., Blewitt, G., Lavallee, D., 2000. On the determination of a global strain rate model. Earth Planets Space 52, 765–770.

Main, I.G., 1996. Statistical physics, seismogenesis, and seismic hazard. Reviews of Geophysics 34, 433–462.

Main, I.G., 2000a. A damage mechanics model for power-law creep and earthquake aftershock and foreshock sequences. Geophysical Journal International 142, 151–161.

Main, I.G., 2000b. Apparent breaks in scaling in the earthquake cumulative frequency–Magnitude distribution: fact or artifact? Bulletin of the Seismological Society of America 90, 86–97.

Main, I.G., Al-Kyndi, F.H., 2002. Entropy, energy, and proximity to criticality in global earthquake populations. Geophysical Research Letters 29, 1121,, doi:10.1029/2001GL014078.

Main, I.G., Irving, D., Musson, R., Reading, A., 1999a. Constraints of frequency–magnitude relation and maximum magnitudes in the UK from observed seismicity and glacio-isostatic recovery rates. Geophysical Journal International 137, 535–550.

Main, I.G., Leonard, T., Papasoulitiotis, O., Hatton, C.G., Meredith, P.G., 1999b. One slope or two? Detecting statistically significant breaks of slope in geophysical data, with application to fracture scaling relationships. Geophysical Research Letters 26, 2801–2804.

Main, I.G., O'Brien, G., Henderson, J.R., 2000. Statistical physics of earthquakes: Comparison of distribution exponents for surface area and potential energy and the dynamic emergence of log-periodic energy quanta. Journal of Geophysical Research 105, 6105–6126.

Marrett, R., 1996. Aggregate properties of fracture populations. Journal of Structural Geology 18, 169–178.

Marrett, R., Allmendinger, R.W., 1990. Kinematic analysis of fault-slip data. Journal of Structural Geology 12, 973–986.

Marrett, R., Allmendinger, R.W., 1991. Estimates of strain due to brittle faulting: sampling of fault populations. Journal of Structural Geology 13, 735–738.

Marrett, R., Peacock, D.C.P., 1999. Strain and stress. Journal of Structural Geology 21, 1057–1063.

Molnar, P., 1983. Average regional strain due to slip on numerous faults of different orientations. Journal of Geophysical Research 88, 6430–6432.

Nemcok, M., Lisle, R.J., 1995. A stress inversion procedure for polyphase fault/slip data sets. Journal of Structural Geology 17, 1445–1453.

Nemcok, M., Kovác, D., Lisle, R.J., 1999. A stress inversion procedure for polyphase calcite twin and fault/slip data sets. Journal of Structural Geology 21, 597–611.

Nieto-Samaniego, A.F., 1999. Stress, strain and fault patterns. Journal of Structural Geology 21, 1065–1070.

Oertel, G., 1965. The mechanism of faulting in clay experiments. Tectonophysics 2, 343–393.

Pollard, D.D., 2000. Strain and stress: discussion. Journal of Structural Geology 22, 1359–1367.

Ranalli, G., 2000. Rheology of crust and its role in tectonic reactivation. Journal of Geodynamics 30, 3–15.

Ranalli, G., Yin, Z.-M., 1990. Critical stress difference and orientation of faults in rocks with strength anisotropies: the two-dimensional case. Journal of Structural Geology 12, 1067–1071.

Reches, Z., 1978. Analysis of faulting in three-dimensional strain field. Tectonophysics 47, 109–129.

Reches, Z., 1983. Faulting of rocks in three-dimensional strain fields II. Theoretical analysis. Tectonophysics 95, 133–156.

Reches, Z., Baer, G., Hatzor, Y., 1992. Constraints on the strength of the upper crust from stress inversion of fault slip data. Journal of Geophysical Research 97, 12.481–12.493.

Rundle, B.J., Turcotte, D.L., Shcherbakov, R., Klein, W., Sammis, C., 2003. Statistical physics approach to understanding the multiscale dynamics of earthquake fault systems. Reviews of Geophysics 41, 1019, doi:10.1029/2003RG000135.

Scholz, C.H., Cowie, P.A., 1990. Determination of total geologic strain from faulting. Nature 346, 837–839.

Schultz, R.A., Fossen, H., 2002. Displacement-length scaling in three dimensions: The importance of aspect ratio and application to deformation bands. Journal of Structural Geology 24, 1389–1411.

Tikoff, B., Wojtal, S.F., 1999. Displacement control of geologic structures. Journal of Structural Geology 21, 959–967.

Turcotte, D.L., 2001. Self-organized criticality: Does it have anything to do with criticality and is it useful? Nonlinear Processes in Geophysics 8, 193–196.

Twiss, R.J., Unruh, J.R., 1998. Analysis of fault slip inversions: Do they constrain stress or strain rate? Journal of Geophysical Research 103, 12,205–12,222.

Udias, A., 1999. Principles of Seismology. Cambridge University Press, Cambridge, 475 pp.

Volant, P., Grasso, J.R., 1994. The finite extension of fractal geometry and power-law distribution of shallow earthquakes: A geomechanical effect. Journal of Geophysical Research 99, 22.879–22.889.

Vrabec, M., Fodor, L., 2006. Late Cenozoic tectonics of Slovenia: structural styles at the north eastern corner of the Adriatic microplate. In: Pinter, N. (Ed.), The Adria Microplate: GPS Geodesy, Tectonics and Hazards. NATO Science Series IV, 61. Earth and Environmental Sciences, pp. 151–168.

Watterson, J., 1999. The future of failure: stress or strain? Journal of Structural Geology 21, 939–948.

Xu, S.-S., Nieto-Samaniego, A.F., Alaniz-Álvarez, S.A., 2006. Effect of sampling and linkage on fault length and length-displacement relationship. International Journal of Earth Science 95, 841–853.

Yamaji, A., 2000a. Multiple inverse method applied to mesoscale faults in mid Quaternary sediments near the triple trench junction off central Japan. Journal of Structural Geology 22, 429–440.

Yamaji, A., 2000b. The multiple inverse method: a new technique to separate stresses from heterogeneous fault-slip data. Journal of Structural Geology 22, 441–452.
Yamaji, A., 2003. Are the solutions of stress inversion correct? Visualization of their reliability and the separation of stresses from heterogeneous fault-slip data. Journal of Structural Geology 25, 241–252.
Yamaji, A., Otsubo, M., Sato, K., 2006. Paleostress analysis using the Hough transform for separating stresses from heterogeneous fault-slip data. Journal of Structural Geology 28, 980–990.
Yin, Z.-M., Ranalli, G., 1992. Critical stress difference, fault orientation and slip direction in anisotropic rocks under non-Andersonian stress systems. Journal of Structural Geology 14, 237–244.
Yin, Z.-M., Ranalli, G., 1995. Estimation of the frictional strength of faults from inversion of fault-slip data: a new method. Journal of Structural Geology 17, 1327–1335.
Žalohar, J., Vrabec, M., 2007. Paleostress analysis of heterogeneous fault-slip data: the Gauss method. Journal of structural Geology 29, 1798–1810.